



**HAL**  
open science

## Spectroscopic Investigation of Nitric Acid Monohydrate

Philipp Baloh, Hinrich Grothe, Karin Whitmore, Stewart F. Parker, Beatriz Martín-Llorente, Rafael Escribano

► **To cite this version:**

Philipp Baloh, Hinrich Grothe, Karin Whitmore, Stewart F. Parker, Beatriz Martín-Llorente, et al.. Spectroscopic Investigation of Nitric Acid Monohydrate. *Molecular Physics*, 2011, pp.1. 10.1080/00268976.2011.593571 . hal-00716636

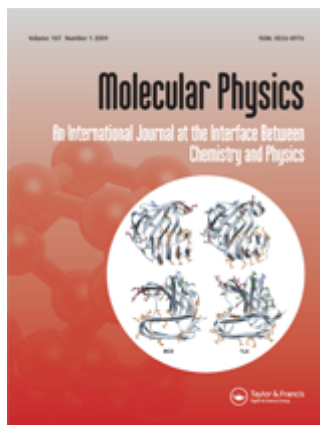
**HAL Id: hal-00716636**

**<https://hal.science/hal-00716636>**

Submitted on 11 Jul 2012

**HAL** is a multi-disciplinary open access archive for the deposit and dissemination of scientific research documents, whether they are published or not. The documents may come from teaching and research institutions in France or abroad, or from public or private research centers.

L'archive ouverte pluridisciplinaire **HAL**, est destinée au dépôt et à la diffusion de documents scientifiques de niveau recherche, publiés ou non, émanant des établissements d'enseignement et de recherche français ou étrangers, des laboratoires publics ou privés.



## Spectroscopic Investigation of Nitric Acid Monohydrate

Journal:	<i>Molecular Physics</i>
Manuscript ID:	TMPH-2011-0090.R1
Manuscript Type:	Special Issue Paper - Dijon HRMS
Date Submitted by the Author:	23-May-2011
Complete List of Authors:	Baloh, Philipp; Vienna University of Technology, Institute of Materials Chemistry Grothe, Hinrich; Vienna University of Technology, Institute of Materials Chemistry Whitmore, Karin; Vienna University of Technology, Universitaere Service-Einrichtung fuer Transmissionselektronenmikroskopie (USTEM) Parker, Stewart; ISIS Facility, STFC Rutherford Appleton Laboratory Martín-Llorrente, Beatriz; IEM-CSIC, Instituto de Estructura de la Materia Escribano, Rafael; IEM-CSIC, Instituto de Estructura de la Materia
Keywords:	IR, Raman spectroscopy, Nitric acid monohydrate, INS

SCHOLARONE™  
Manuscripts

## Spectroscopic Investigation of Nitric Acid Monohydrate

Philipp Baloh,<sup>a</sup> Hinrich Grothe,<sup>\*a</sup> Karin Whitmore,<sup>b</sup> Stewart F. Parker,<sup>c</sup>  
Beatriz Martín Llorente,<sup>d</sup> and Rafael Escribano<sup>d</sup>

Deleted:

<sup>a</sup> Vienna University of Technology, Institute of Materials Chemistry, [Getreidemarkt 9/BC/165](#), 1060 Vienna, Austria. Fax: +43 1 58801 165980; Tel: +43 1 58801 165122; E-mail: [grothe@tuwien.ac.at](mailto:grothe@tuwien.ac.at)

Deleted: Leurgasse 2-4

<sup>b</sup> Vienna University of Technology, Universitaere Service-Einrichtung fuer Transmissionselektronenmikroskopie (USTEM), Wiedner Hauptstr. 8, 1040 Vienna, Austria. Fax: +43 1 58801 13898; Tel: +43 1 58801 13728; E-mail: [ustem@ustem.tuwien.ac.at](mailto:ustem@ustem.tuwien.ac.at)

<sup>c</sup> ISIS Facility, STFC Rutherford Appleton Laboratory, Chilton, Didcot, Oxon, OX11 0QX, United Kingdom. Fax: +44 1235 445720; Tel: +44 1235 446182; E-mail: [stewart.parker@stfc.ac.uk](mailto:stewart.parker@stfc.ac.uk)

<sup>d</sup> Instituto de Estructura de la Materia, IEM-CSIC, Serrano 123, 28006, Madrid, Spain. Fax: +34 915855184; Tel: +34 915901609; E-mail: [Rafael.escribano@csic.es](mailto:Rafael.escribano@csic.es)

### Abstract

Vibrational spectroscopy, X-ray diffraction, and electron microscopy have been applied to investigate the crystallization of concentrated amorphous nitric acid ( $0.5 \leq x \leq 0.95$ ). Crystalline nitric acid monohydrate ( $\text{HNO}_3 \cdot \text{H}_2\text{O}$ ) is the major hydrate phase detected together with traces of metastable nitric acid dihydrate ( $\text{HNO}_3 \cdot 2\text{H}_2\text{O}$ ) and pure crystalline nitric acid. Nitric acid tetrohydrate ( $4\text{HNO}_3 \cdot \text{H}_2\text{O}$ ) was not achievable. The diffraction data show [nitric acid monohydrate](#) as a highly symmetrical structure, which bestows clearly laid out infrared, Raman and inelastic neutron scattering spectra. The low frequency region is still a matter of discussion since experiment and theory are not in accordance. The microscopic picture underlines the model character of [nitric acid monohydrate](#), since the crystalline particles **adopt a spherical shape, on various agglomeration stages**, which minimizes the interference of scattering on the spectroscopic data.

Deleted: (INS)

## Introduction

Nitric acid monohydrate (NAM) has been a subject of research for many different reasons over the years. The first publications concerning NAM were written in 1951 by Luzzati who solved the structure of solid NAM by single-crystal X-ray diffraction (XRD).<sup>1</sup> At [that](#) time, the interest was purely academic and the structures of several acids and their hydrates were solved in a similar way. In 1953 Bethell and Sheppard monitored solid and liquid NAM by IR-spectroscopy.<sup>2</sup> 15 years later, Janik *et al.* published the first inelastic neutron scattering (INS) experiments on solid NAM and other similar hydrates.<sup>3,4</sup> They compared their results with existing IR and Raman data. A particular focus was on the low-frequency region. In 1974, Dawber carried out vapour pressure experiments with liquid HNO<sub>3</sub> in the concentration region of NAM, in order to prove the stability of H<sub>3</sub>O<sup>+</sup> and NO<sub>3</sub><sup>-</sup> ions.<sup>5</sup> Delaplane *et al.* studied the hydrogen bonds of these NAM constituents using XRD and *ab initio* calculations.<sup>6</sup> A subsequent paper of Janik *et al.* appeared in 1978, observing also the INS spectra of amorphous NAM and its crystallization changes.<sup>7</sup> For a closer inspection of the amorphous state, in 1979 Herzog-Cance *et al.* analyzed the glass form of NAM as well as its changes during crystallization using fast Raman and wide-line NMR spectroscopy.<sup>8</sup>

In the early 1980s a decrease of the earth ozone layer was predicted and in 1985 a seasonal ozone depletion in the lower polar stratosphere was observed.<sup>9,10</sup> In the following years much research was focused on polar stratospheric clouds (PSCs), which play a central role in heterogeneous stratospheric chemistry. Thus, the micro-physical mechanisms of PSC formation became an important issue. Nitric acid hydrates (NAX) were found to be the major constituents of PSCs.<sup>11</sup> These findings prompted the gathering of abundant information about the NAX species, including NAM. In this context, Hanson and Mauersberger presented their study of NAM,<sup>12</sup> in which they also measured the vapour pressure over nitric acid mono- and trihydrate. Over the years several groups published infrared and Raman data of NAX comparing the features of the mono-, di- and trihydrate during different annealing procedures.<sup>13-19</sup> This information was complemented by cluster experiments, kinetic measurements, *ab initio* calculations, and XRD studies.<sup>20-26</sup> Particularly for the purposes of heterogeneous chemistry, surface spectra of nitric acid hydrates were recorded using diffuse reflectance spectroscopy (DRIFTS), sum frequency

1  
2 generation (SFG), and grazing-angle reflection absorption infrared spectroscopy  
3 (RAIRS).<sup>22,27-32</sup> These surface investigations showed molecular HNO<sub>3</sub> to be present  
4 on the surface of NAM films. For comparison with field measurements the optical  
5 constants of nitric acid hydrates were determined.<sup>33</sup>  
6  
7

8 Today it is generally accepted that NAM has no real relevance in the micro-physics  
9 of PSCs because of the moderate concentration of nitric acid found at this altitude.  
10 However, the research on NAM carried on for another reason. Theoretical chemists  
11 discovered that NAM is a good model substance because it is simpler to calculate  
12 than any other hydrate and there already exists abundant information which can be  
13 used to test these calculations. During the last 15 years many investigations have  
14 been carried out to develop improved theoretical models.<sup>21,22,34-39</sup> Only recently the  
15 X-ray diffraction data have been re-investigated by Lebrun *et al.*<sup>40</sup> improving the  
16 known structure and Walker *et al.*<sup>39</sup> have determined the behaviour of NAM up to a  
17 pressure of 43 kbar where three different structural phases have been identified.  
18  
19

20 **This paper aims to provide a more comprehensive picture of the structure and**  
21 **spectroscopic properties of NAM. To this end, we present new morphological**  
22 **information from environmental scanning electron microscopy (ESEM) and X-ray**  
23 **diffraction measurements, together with improved INS spectra. In addition, new IR**  
24 **and Raman data, with their spectroscopic analysis, are also given. The article is**  
25 **structured as follows. First, the experimental details of all techniques employed, are**  
26 **described. Next, the results attained by each technique are presented and discussed.**  
27 **The conclusions are outlined in a final section.**  
28  
29

30 In the present paper, new spectroscopic data (FTIR, Raman and INS) and high level  
31 quantum chemical calculations are collected. These data are additionally correlated  
32 with morphological information from environmental scanning electron microscopy  
33 (ESEM).  
34  
35

## 36 **Experimental**

37 Specific sample preparation methods of NAM depended on the experimental analysis  
38 tool to be used. But all ways of preparation were based on concentrated solutions of  
39 HNO<sub>3</sub> in H<sub>2</sub>O. These solutions were quenched by different methods always with the  
40 aim to produce an amorphous sample, which was consequently crystallized in the  
41 course of an annealing program which included the following steps:  
42  
43  
44  
45  
46  
47  
48  
49  
50  
51  
52  
53  
54  
55  
56  
57  
58  
59  
60

1  
2 (I) the amorphous sample was heated ( $5 \text{ K min}^{-1}$ ) to a temperature above the glass  
3 transition point,  
4

5 (II) the sample was kept at the constant temperature of interest until repeated short-term  
6 measurements, revealed no further changes,

Deleted:

7  
8 (III) the sample was cooled back to a temperature below the glass transition point (125  
9 K) and a long-term measurement was started.  
10

11 Structural changes in the course of the subsequent thermal treatment were observed by  
12 X-ray diffraction, FTIR, Raman and INS spectroscopy. Additionally, environmental  
13 scanning electron microscopy was applied to a NAM sample to gain information about  
14 its morphology.  
15

16  
17 The set up for the XRD measurements was the same as that described in ref. 23 and 41  
18 and therefore, it will only be discussed in brief here. It consists of three parts: an aerosol  
19 chamber, a sample compartment, and a high vacuum (HV) cryostat. To form the aerosol  
20 a Meinhardt<sup>®</sup> nebulizer (TR-50A1) was used to disperse the nitric acid solution. A  
21 Teflon slide separates the sample compartment from the high vacuum part with the  
22 colder surfaces of the cryostat. Thus, the sample may be kept under its own vapour  
23 pressure without any sample transfer to the cold cryostat surfaces. The sample support  
24 (gold plated aluminium) is mounted at the cold end of a helium closed-cycle cryostat  
25 (RGD 210 Leybold, Germany) which is located in the centre of a two cycle goniometer  
26 in Bragg-Brentano  $\theta$ - $\theta$ -geometry (3000TT Seifert, Germany). Ni-filtered copper  
27 radiation ( $\lambda_1(\text{Cu-K}\alpha_1)$ :  $1.54051 \text{ \AA}$ ;  $\lambda_2(\text{Cu-K}\alpha_2)$ :  $1.54433 \text{ \AA}$ ) illuminates the sample  
28 through an aperture closed with a metalized Mylar foil of  $40 \mu\text{m}$  thickness. The  
29 scattered rays were collected by a scintillation counter.  
30

31  
32 The FTIR set-up was specially designed to protect its sensitive optical components  
33 in the course of quenching the aggressive mixtures. A detailed description of the  
34 apparatus can be found in the work of Tizek et al.<sup>41</sup> The HV-cryostat chamber can be  
35 separated by a gate valve into a measurement chamber inside and a sampling  
36 compartment outside the spectrometer. An edge welded bellows with a jounce travel  
37 of  $200 \text{ mm}$  permits the sample support to be moved from one position to the other  
38 without any deterioration of the vacuum conditions. Spectra were recorded by co-  
39 addition of 10 scans at a resolution of  $4 \text{ cm}^{-1}$  with a Bruker 113v spectrometer  
40 (Karlsruhe/Germany). The IR-beam was focused on the gold plated sample support  
41 where the sample was analyzed in double transmission. Cooling was performed via  
42 dry air which was precooled to  $80 \text{ K}$  by heat exchange with liquid nitrogen. The  
43  
44  
45  
46  
47  
48  
49  
50  
51  
52  
53

1  
2 coolant flowed into the sample carrier in the inner one of two concentric tubes and  
3 left the cryostat via the outer one. Thus a minimum temperature of less than 90 K is  
4 achieved. A temperature sensor (thermocouple) is located in an orifice directly  
5 below the carrier surface. Its accuracy could be determined by analyzing the vapor  
6 pressure of water and the  $\alpha$ -/ $\beta$ -transition of cyclohexane and it amounted to  $\pm 1$  K.  
7 FTIR measurements require only a few seconds' time and spectra could be taken  
8 throughout the thermal treatment of the sample.

9  
10 The preparation techniques for ESEM differ somewhat from the others. While in the  
11 case of XRD and FTIR an aerosol was deposited, for ESEM a droplet of approximately  
12 4  $\mu$ l was quenched in a liquid nitrogen bath. To analyze the NAM sample the method of  
13 freeze fracturing proved to be very useful. A sample carrier with a hole was filled with  
14 the liquid sample thus producing a drop that projected above the hole. Then the sample  
15 carrier with the sample was quenched in liquid nitrogen and transferred to the  
16 preparation chamber of the ESEM. In the preparation chamber all parts were cooled  
17 with liquid nitrogen to a temperature of about 110 to 125 K. The portion of the sample  
18 drop which lay above the sample carrier was broken away by a cold edge of a weld  
19 manipulator. The so-gained surface is clean and virgin and enables a very good analysis  
20 of the sample. Environmental scanning electron microscopy (ESEM) can be operated at  
21 higher pressures than traditional SEM. The NAM sample was observed under the  
22 pressure of an imaging gas ( $N_2$ ) thus preventing the sample from evaporating. The  
23 measurements were done on a FEI Quanta 200 3D DBFIB at the University Service  
24 Centre for Transmission Electron Microscopy (USTEM) at the Vienna University of  
25 Technology. The annealing process was initiated in this case by stepwise heating the  
26 cryo-stage in the ESEM to the desired temperature. This procedure allows taking  
27 pictures while manipulating the temperature of the sample.

28  
29 The production of samples for Raman spectroscopy was quite simple. For this purpose  
30 small glass capillaries (outer diameter 2 mm, wall thickness 0.5 mm, length 15 mm)  
31 were filled with 4  $\mu$ l nitric acid solution (50 mol%). After the capillary was filled it was  
32 dipped into a liquid nitrogen bath where the sample froze to give an amorphous solid.  
33 This worked very well and was reproducible due to the very efficient heat exchange.  
34 The capillary containing the sample was then transferred into a cryostat where a  
35 temperature of 140 K was maintained by a cold nitrogen gas stream. The detailed  
36 description of this cryostat can be found elsewhere.<sup>42</sup> The annealing could be done with  
37 a heating rate of approximately 5 K  $min^{-1}$ . The spectra were recorded using a Dilor

Deleted:

1  
2 RTI30 spectrometer equipped with an argon ion laser (514.5nm). The laser was guided  
3 through the double walled glass cryostat onto the sample capillary and the scattered  
4 light was collected perpendicular to the incident laser.  
5

6 The INS measurements were carried out using TOSCA<sup>43</sup> spectrometer at the ISIS  
7 Facility.<sup>44</sup> TOSCA offers high resolution,  $\sim 1.25\% \Delta E/E$  between 16 and 4000  $\text{cm}^{-1}$ . The  
8 cryostat on TOSCA consists of a single stage closed cycle refrigerator (CCR, [Leybold](#))  
9 that cools an outer radiation shield to  $\sim 45$  K and two dual stage 4 K CCRs (Sumitomo)  
10 that cool a central chimney, at the bottom of which the sample is mounted on the end of  
11 a special pole, a centrestick. (The neutron beam passes through the lower part of a  
12 cryostat.) The sample is cooled by [convection](#) across a low pressure, 20 mbar, of helium  
13 exchange gas. To change sample, the chimney is filled with helium gas to atmospheric  
14 pressure, the centrestick withdrawn and exchanged for another with the next sample  
15 attached. The chimney is then evacuated to its operational pressure and the sample  
16 allowed to cool. The sample changeover can easily be accomplished in less than half-  
17 an-hour and the sample cools to base temperature ( $\sim 12$  K) in about two hours.  
18 For the sample preparation small droplets of about 4  $\mu\text{l}$  were quenched one after another  
19 directly in a liquid nitrogen bath. After that they were transferred onto the sample  
20 carrier still under liquid nitrogen. During this procedure the uttermost care was needed  
21 not to touch the sample with any parts that had not been cooled to liquid nitrogen  
22 temperature to avoid partial crystallization of the amorphous sample. The sample carrier  
23 was then transferred quickly out of the nitrogen bath into the cryostat of the TOSCA  
24 apparatus which had a temperature of approximately 20 K. Then the analysis was  
25 started. A spectrum at 20 K was first recorded to ensure the amorphicity of the sample.  
26 In the annealing procedure the NAM sample was heated to 180 K, cooled down, and  
27 finally the spectrum of the crystallized phase was recorded.  
28  
29  
30  
31  
32  
33  
34  
35  
36  
37  
38  
39  
40

## 41 Results

### 42 [XRD data](#)

43 Nitric acid monohydrate crystallizes in the orthorhombic space group  $P2_1cn$  with  
44 cell parameters  $a=6.317$  (3)  $\text{\AA}$ ,  $b=8.723$  (4)  $\text{\AA}$  and  $c=5.477$   $\text{\AA}$  (see [Figure 1](#)).<sup>40</sup> The  
45 crystallographic data [were](#) used for calculating the powder diffractogram, shown at  
46 top of [Fig. 2a](#) as a bar diagram, in comparison with an experimental diffractogram of  
47 the 1:1 stoichiometry mixture. There is ample accordance, not only in signal  
48 positions but also in the relation of reflections' intensities ([not evident in the bar](#)  
49  
50  
51  
52  
53  
54  
55  
56  
57  
58  
59  
60

1  
2 | [diagram shown here](#)). Disturbing influences like texture effects appear only to a very  
3 | minor extent and do not affect the present analysis, which makes further refinement  
4 | unnecessary.  
5  
6  
7

### 8 9 **Figure 1**

10  
11 | The diffractograms in Figure [2a](#) exhibit a clearly observable phase transition from  
12 | amorphous to crystalline NAM starting at about 154 K, which is 4 K above the glass  
13 | transition point of the sample.<sup>45</sup> In general, the diffractogram of an amorphous  
14 | sample is unstructured and exhibits a broad intensity distribution about a wide angle  
15 | range. [In addition to the signal from the sample](#), there is also a signal from the  
16 | cryostat itself, which results from the windows material and the sample carrier.  
17 | During crystallization the respective reflections grow upon this background.  
18  
19

### 20 21 **FTIR data**

22  
23 | Whereas X-ray diffraction [data](#) supply the fundamental information of a phase  
24 | transition, i.e. a change in the long-range order of the sample structure, vibrational  
25 | spectroscopy can furnish information on the short-range order structural changes  
26 | occurring during this phase transition. In Figure [2b](#) there are three main frequency  
27 | regions where changes become most obvious:  
28  
29

- 30  
31  
32 • Between 3300 and 3000  $\text{cm}^{-1}$  the typical absorptions of the OH-stretching  
33 | vibrations of water disappear during crystallization.  
34  
35 • Conversely, strong bands at 2644 and 2226  $\text{cm}^{-1}$  grow in the same process. These  
36 | bands can be associated with  $\nu_1$  and  $\nu_3$  of  $\text{H}_3\text{O}^+$  whereas the emerging bands at 1663  
37 |  $\text{cm}^{-1}$  and 1116  $\text{cm}^{-1}$  are assigned to  $\nu_4$  and  $\nu_2$  of the same cation, respectively.<sup>36</sup>  
38  
39 • A strong absorption at 1238  $\text{cm}^{-1}$  can be assigned to the [anti](#)symmetric stretching  
40 | band of  $\text{NO}_3^-$ . The symmetric stretching band  $\nu_1(\text{NO}_3^-)$  is infrared inactive. It is not  
41 | observed at 1050  $\text{cm}^{-1}$ , [but](#) it does appear in the spectra of other nitric acid hydrates,  
42 | sometimes as a split feature, revealing an asymmetric environment of the nitrate  
43 | group.  
44  
45

46  
47 | Thus, the infrared spectrum provides evidence that in the amorphous sample (lowest  
48 | trace in Fig. [2b](#)), dissociation of the acid is not complete, and the neutral species  
49 | coexist with a partial concentration of the ions. In addition, trace amounts of  $\text{N}_2\text{O}_4$   
50 | have been trapped and detected (1742 and 1761  $\text{cm}^{-1}$ ). This dimer is formed due to  
51  
52

the decomposition of nitric acid vapor (the partial pressure of which is ~14 mbar above the solution), and is observed thanks to the strong absorption intensity of these bands in the dimer. After crystallization, nitric acid monohydrate exhibits a complete dissociation into  $\text{NO}_3^-$  and  $\text{H}_3\text{O}^+$  as shown in the crystallographic scheme of Figure 1, where no molecular  $\text{HNO}_3$  is present. All constituents are dissociation products and all oxygen and hydrogen atoms are connected via hydrogen bonds within each layer. Every oxonium ion is linked to three planar nitrate ions. In this manner, layers of nitrate and oxonium are built up, being interconnected to each other by weak van der Waals forces.

Deleted: infinite

### Figure 2

Higher  $\text{HNO}_3$  concentrations, with  $0.5 < x < 0.95$ , have also been investigated. Pure nitric acid and NAM crystallize according to the respective stoichiometry, as expected from the phase diagram.<sup>46, 47</sup> Traces of  $\alpha$ -NAD (phase I) appear due to the non-equilibrium conditions when crystallizing from the amorphous sample.<sup>23, 48</sup> With increasing concentration, the point of nitric acid crystallization drops below the of NAM. Figure 3 displays results for a nitric acid concentration of 54 mol%.

Deleted: (NA)

Deleted: <sup>45</sup>

Deleted: one

The presence of crystalline nitric acid is confirmed by a XRD reflection at  $26.3^\circ$  (Fig. 3, grey field). During annealing, the pure nitric acid starts to melt at the eutectic temperature of 208 K yielding NAM and the liquid phase (Fig. 3, 210 K, top trace). Finally, it must be stated that no signs have been found for the existence of a tetrahydrate  $4\text{HNO}_3 \cdot \text{H}_2\text{O}$  ( $x=0.83$ ) which has been postulated based on differential scanning calorimetry, Raman spectroscopy, and vapour pressure measurements.<sup>49, 50</sup> In the test described here there are no other important changes besides the disappearance of the nitric acid signal (labeled NA) above the eutectic point at 208 K. The monohydrate melts in accordance to the literature phase diagram at around 235 K.

Deleted: <sup>46</sup>Deleted: <sup>47</sup>

### Figure 3

Undiluted nitric acid ( $x \sim 0.95$ ) has been investigated as well but could not be frozen out fully amorphously: Several sharp and intense reflections appear on the

1  
2  
3  
4  
5  
6  
7  
8  
9  
10  
11  
12  
13  
14  
15  
16  
17  
18  
19  
20  
21  
22  
23  
24  
25  
26  
27  
28  
29  
30  
31  
32  
33  
34  
35  
36  
37  
38  
39  
40  
41  
42  
43  
44  
45  
46  
47  
48  
49  
50  
51  
52  
53  
54  
55  
56  
57  
58  
59  
60

unspecific background of the amorphous fraction (diffractogram not shown). The [nitric acid](#) ambient-pressure phase I has been identified unambiguously.<sup>51</sup> Neither from the diffractograms nor from the IR spectra can the ratio between amorphous and crystalline structures be derived. Obviously, pure [nitric acid](#) has a very low glass transition point.<sup>45</sup> Crystallization of [nitric acid](#) already proceeds below 150 K. Therefore, measurements above 160 K rarely show any differences. Minor parts of the diffractogram show accordance with the diffraction pattern of NAM, the development of which indicates a slight crystalline impurity in the phase composition. The water of the NAM structure originates from the dissociation of HNO<sub>3</sub> into H<sub>2</sub>O and NO<sub>2</sub>. Traces of N<sub>2</sub>O<sub>4</sub> are detectable in the IR spectrum.

### INS data

The spectrum labelled with 20 K in [Fig. 4](#) is the first spectrum taken just after the sample was loaded into the cryostat, following the protocol described in the experimental part. At this stage, the sample is amorphous and has not been annealed yet. The spectrum largely resembles that of strongly disordered water found on metal [oxides](#)<sup>52-55</sup> and is assigned similarly: water translational and librational modes [from 0 to 300 cm<sup>-1</sup>](#) and [from 300 to 1100 cm<sup>-1</sup>](#), respectively, and the H–O–H scissors vibration at ~1600 cm<sup>-1</sup>. The O–H stretching modes are not seen on TOSCA because the momentum transfer,  $Q$  (Å), and the energy transfer,  $E_t$  (cm<sup>-1</sup>) are related by  $Q^2 \sim E_t/16$  and thus for large energy transfer,  $Q$  is also large and all the spectral intensity lies in the phonon wings (combinations of the internal modes and the external density of states), and as a result the high-frequency fundamentals are not observed.<sup>56</sup> The only evidence for the presence of nitric acid is the peak at ~1430 cm<sup>-1</sup> assigned to the N–O–H bend.

As expected from the phase diagram and shown by XRD ([Fig. 2a](#), trace (2)), the amorphous 50 mol% nitric acid solution is fully converted into NAM, the only phase to crystallize, upon annealing to 180 K. Immediately after tempering for 30 minutes, the sample was fast cooled to 20 K. Since the amorphous/crystalline phase transition is irreversible, the measurement could be carried out at 20 K without interference. A spectrum with many intense narrow bands is thus recorded ([Fig. 4](#), trace 2) and the difference to the spectrum of the amorphous phase (trace 1) is striking.

Our high resolution INS spectrum allows resolving broad structures as seen in the previous low resolution INS measurements by Janik *et al.*<sup>3</sup>. For example, the broad

Deleted: in

Deleted: state

Deleted: -

Deleted: -

1  
2 feature at  $758\text{ cm}^{-1}$  observed by these authors is decomposed into at least six  
3 different bands in our work.

4  
5 The uppermost [calculated](#) spectrum (trace 3) [was](#) generated from a previously  
6 reported<sup>37</sup> DFT calculation by the program ACLIMAX.<sup>57</sup> Inspection of the  
7 eigenvectors shows that the INS spectrum is dominated by modes involving the  
8  $\text{H}_3\text{O}^+$  ion and can be divided into [four](#) regions: translational modes [from 0 to 300](#)  
9  $\text{cm}^{-1}$ , librational modes [from 600 to 900](#)  $\text{cm}^{-1}$ , H–O–H bending modes [from 900 to](#)  
10  $1700\text{ cm}^{-1}$  and overtones and combinations at  $> 1700\text{ cm}^{-1}$ . It can be seen that the H–  
11 O–H bending modes are reasonably well described, the librational modes are  
12 calculated somewhat higher than observed and the translational modes, shown in  
13 more detail in [Fig. 5](#), are poorly represented by the calculation.

14  
15 The reduced agreement between the observed and calculated INS spectra in the low-  
16 frequency region arises from the choice of model employed. The energies and  
17 vibrational modes are calculated at the  $\Gamma$ -point (*i.e.* at wavevector  $\kappa=0$ ) in the  
18 Brillouin zone, where infrared and Raman modes are allowed. In contrast, INS  
19 spectroscopy is sensitive to all wavevectors across the complete Brillouin zone. In  
20 cases where there is little or no dispersion in the modes there is usually good  
21 agreement between a  $\Gamma$ -point calculation and the observed spectra.<sup>56</sup> That this is not  
22 the case for the present study [but](#) is strong evidence that there is significant  
23 dispersion in the modes. Hydrogen-bonded systems are well known to exhibit  
24 dispersion and the present example is a textbook case where such effects would need  
25 to be considered to accurately model the INS spectrum. Unfortunately, such a  
26 calculation is beyond our available resources.

#### Figure 4

27  
28 The low-frequency region is enlarged in [Fig. 5](#) where the calculated IR spectrum and  
29 the observed INS and Raman spectra (traces 1 to 3 respectively) are shown. The  
30 sample for the Raman spectrum was prepared in the way described above (ref. 19).  
31 All three spectra seem different at first glance, as corresponding to the diverse  
32 techniques used in each case. All vibrations where hydrogen is involved produce a  
33 strong signal in the INS spectrum, whereas in the Raman spectrum all vibrations  
34 which involve the movement of an oxygen atom are more intense due to the  
35 favoured change in polarizability, related to the higher electron density on oxygen

atoms. The spectral features represented in Fig. 5 are listed in Table 1, with previous INS data and a tentative assignment of some modes. Some agreement can be found, especially in band positions, in the two regions alternatively covered by Raman observations and IR predictions. In the Raman and lower frequency part of the INS spectra, the two most prominent features seem correlated, with a small red shift in the Raman. In the higher frequency spectral region of the figure, the peak at  $\sim 320 \text{ cm}^{-1}$  is present in both the INS and the predicted IR spectra, whereas the neutron scattering bands in the  $200$  to  $250 \text{ cm}^{-1}$  zone seem to be more spread in the calculated infrared trace. Atomic displacements per normal mode derived in the calculations indicate that most of these vibrations can be described as in-phase and out-of-phase twisting of the  $\text{NO}_3^-$  group and flattening of  $\text{H}_3\text{O}^+$ .

### Figure 5

Table 2 presents a summary of previous and current assignments in the region between  $600$  and  $1700 \text{ cm}^{-1}$ , covered by the INS measurements, as shown in Fig. 4. In general terms, there is a reasonably good agreement among all series of IR measurements and with the present INS spectra. The strongest INS bands correspond to vibrations of the oxonium ion: torsion, symmetric bending and asymmetric bending, at  $\sim 750 \text{ cm}^{-1}$ ,  $1130 \text{ cm}^{-1}$  and  $1670 \text{ cm}^{-1}$  respectively, whereas the strongest IR bands are those assigned to the asymmetric stretching of the  $\text{NO}_3^-$  ion, at  $1315 \text{ cm}^{-1}$ .

**Table 1.** Low frequency vibrations (in  $\text{cm}^{-1}$ ) of NAM

INS <sup>a</sup>	IR <sup>b</sup>	Raman <sup>c</sup>	INS <sup>d</sup>	Assignment <sup>e</sup>
59		58		
70		75		
90		86		
		101		
124		118	112	
135		129		
154		143		
162			164	
203	195		206	Tz
216				
238	234			
249	268		246	Ty
300	304			
318	320(sh)		321	Tx+Tz
387				
421				

<sup>a</sup> INS data from this work, <sup>b</sup> IR calculations by Escribano et al.<sup>59</sup>, <sup>c</sup> Raman data by Grothe et al.<sup>19</sup>, <sup>d</sup> INS data from Janik et al.<sup>4</sup>, <sup>e</sup> assignments by Janik et al.<sup>4</sup>

Deleted:<sup>55</sup>

**Table 2:** Vibrational spectroscopy data of NAM in the mid-IR region (in  $\text{cm}^{-1}$ )

INS <sup>a</sup>	IR <sup>b</sup>	IR <sup>c</sup>	IR <sup>d</sup>	IR <sup>e</sup>	Raman <sup>f</sup>	INS <sup>g</sup>	Assignment <sup>h</sup>
603							
673		675	670	680			(H <sub>3</sub> O <sup>+</sup> ) tors.
	702	700		702			v <sub>L</sub> (H <sub>3</sub> O <sup>+</sup> )
718	721	723	723	722			v <sub>4</sub> (NO <sub>3</sub> <sup>-</sup> ) δ <sub>as</sub>
	735	737	738	735			v <sub>4</sub> (NO <sub>3</sub> <sup>-</sup> ) δ <sub>as</sub>
750						758	(H <sub>3</sub> O <sup>+</sup> )Rz+Ry
770	780			775			
798	814	815	816	813			v <sub>2</sub> (NO <sub>3</sub> <sup>-</sup> ) δ <sub>s</sub>
877							
926							
969							calc.(NO <sub>3</sub> <sup>-</sup> ) v <sub>1</sub>
					1044		
					1055		
1103	1102						
1114				1115			v <sub>2</sub> (H <sub>3</sub> O <sup>+</sup> ) δ <sub>s</sub>
1131	1135	1135	1134				
	1279			1260			v <sub>3</sub> (NO <sub>3</sub> <sup>-</sup> ) v <sub>as</sub>
1314				1316			v <sub>3</sub> (NO <sub>3</sub> <sup>-</sup> ) v <sub>as</sub>
1327							
1402		1386	1361				
1423							
1437							
1459							
1669	1674	1680	1671	1671			v <sub>4</sub> (H <sub>3</sub> O <sup>+</sup> ) δ <sub>as</sub>

<sup>a)</sup> INS data from this work, <sup>b)</sup> IR data by Ritzhaupt and Devlin<sup>13</sup>, <sup>c)</sup> IR data by Savoie and Giguere<sup>56</sup>, <sup>d)</sup> IR data by Bethell and Sheppard<sup>2</sup>, <sup>e)</sup> IR data by Smith et al.<sup>14</sup>, <sup>f)</sup> Raman data by Grothe et al.<sup>19</sup>, <sup>g)</sup> INS data by Janik et al.<sup>4</sup>, <sup>h)</sup> the assignments are summarised from the different sources mentioned in the table.

### ESEM data

During the laborious preparation of the sample outside and inside the microscope (see experimental section), the sample temperature was scrupulously kept below 125 K, which is 30 K beneath the glass transition point of NAM. Thus, an amorphous state can be guaranteed when comparing with XRD and spectroscopic data. During the annealing the electron beam intensity was reduced in order to avoid damage to the sample or the initiation of an uncontrolled crystallization. Microscope pictures of high resolution were recorded only after re-cooling to  $T \leq 125$  K.

### Figure 6

1  
2  
3  
4 In [Figure 6](#) the picture (a) shows an unstructured surface, which is in accordance  
5 with the assumption of a fully amorphous sample. In the pictures (b-d) the ongoing  
6 growth of the crystalline particles can be seen. After 10 minutes small spherical  
7 particles (~200 nm in diameter) can be detected ([Fig. 6b](#)). Ten minutes later ([Fig.](#)  
8 [6c](#)), the spheroids have increased their diameter by a factor of 5 (i.e. a growth rate of  
9 80 nm min<sup>-1</sup>), which corresponds to a volume gain of 125 in 10 minutes. [This panel](#)  
10 [shows a mixture of particles at different stages in their growing process.](#) After a  
11 further 10 minutes interval, the spheroids have merged forming a flocculated carpet of  
12 NAM ([Fig. 6d](#)), [in which individual spherical particles can still be detected on the](#)  
13 [surface of the structure.](#)

## 20 21 Conclusions

22  
23  
24 NAM has been crystallized from various concentrated nitric acid solutions under  
25 extremely non-equilibrium conditions. Only one NAM phase (I) has been observed  
26 at low temperature and at ambient pressure, the same phase (I) achieved at 11 kbar,  
27 as stated in the literature,<sup>39</sup> while the two further NAM phases (II, III) are only  
28 accessible at much higher pressure (42 and 43 kbar). Clearly, they cannot be  
29 generated by any non-equilibrium conditions at ambient pressure.

30 Spectroscopy and diffraction experiments indicate the presence of pure HNO<sub>3</sub> in the  
31 amorphous samples, in accordance with previous SFG, DRIFTS, and RAIRS data  
32 and theoretical studies.<sup>60, 61</sup> The reasons for that are, on one hand, demixing  
33 according to the phase diagram, and on the other hand, the elevated vapour pressure  
34 of HNO<sub>3</sub> above the liquid. Molecular nitric acid is stabilized due to solvation but it  
35 tends to decompose into water and NO<sub>2</sub>, which has also been observed by  
36 spectroscopic means. The present INS data exhibit a much higher quality and better  
37 spectral resolution than the literature data,<sup>3, 4</sup> and have allowed to resolve some new  
38 band positions of water torsions and oxonium hindered rotations.

39 The ESEM pictures presented here provide unprecedented detail of the structure of  
40 NAM, which appears to be formed by spherical crystalline particles [in various stages](#)  
41 [of agglomeration.](#) This conclusion applies to samples grown on a gold support,  
42 whereas air-transported particles might be different. However, if we assume a  
43  
44  
45  
46  
47  
48  
49  
50  
51  
52

spherical morphology of the particles then this is a rather ideal case for vibrational spectroscopy, since Mie scattering of aspherical particles would have distorted the transmission spectra particularly in the region of the stretching bands.<sup>62</sup>

NAM and NAT are the only thermodynamically stable hydrate phases of the nitric acid/water phase diagram. However, from the viewpoint of stratospheric chemistry NAM has only minor relevance because the HNO<sub>3</sub> concentration in atmospheric aerosols at stratospheric altitude does not reach an elevated value. In non-equilibrium processes, NAM could also be formed through the disproportionation of NAD which would produce metastable NAM crystallites.

### Acknowledgments

This research project has been supported (in part) by the European Commission under the 7th Framework Programme through the Key Action: Strengthening the European Research Area, Research Infrastructures. Contract n°: CP-CSA\_INFRA-2008-1.1.1 Number 226507-NMI3. The STFC Rutherford Appleton Laboratory is thanked for access to neutron beam facilities. SFP is grateful for a lecture invitation by the Austrian Chemical Society (GÖCh). RE and BML acknowledge funding from the Spanish Ministry of Education, Project FIS2007-61686.

### References

- 1 V. Luzzati, *Acta Cryst.*, 1951, **4**, 239.
- 2 D. E. Bethell, N. Sheppard, *Journal of Chemical Physics*, 1953, **21**, 1421.
- 3 J. M. Janik, A. Jerzy, A. Bajorek, K. Parlinski, M. Sudnik-Hryniewicz, *Physica*, 1967, **35(4)**, 457.
- 4 J. A. Janik, A. Bajorek, J. M. Janik, I. Natkaniec, K. Parlinski, M. Sudnik-Hryniewicz, *Acta Physica Polonica*, 1968, **33(3)**, 419.
- 5 J. G. Dawber, *Journal of Inorganic and Nuclear Chemistry*, 1975, **37(4)**, 1043.
- 6 R. G. Delaplane, I. Taesler, I. Olovsson, *Acta Crystallographica Section B: Structural Crystallography and Crystal Chemistry*, 1975, **B31(5)**, 1486.
- 7 J. M. Janik, J. MA Janik, A. Bajorek, K. Parlinsk., M. Sudnikhr, *Physica*, 1967, **35(4)**, 457.
- 8 M. H. Herzog-Cance, J. Potier, A. Potier, J. M. Beny, B. Sombret, F. Wallart, *Advances in Molecular Relaxation and Interaction Processes*, 1979, **15(1)**, 1.
- 9 M. J. Molina, F. S. Rowland, *Nature*, 1974, **249**, 810.
- 10 R. S. Stolarski, A. J. Krueger, M. R. Schoeberl, R. D. McPeters, P. A. Newman, J. C. Alpert, *Nature*, 1986, **322**, 808.
- 11 P. J. Crutzen, F. Arnold, *Nature*, 1986, **324**, 651.
- 12 D. Hanson, K. Mauersberger, *Geophysical Research Letters*, 1988, **15(8)**, 855.

Deleted: t

Formatted: Bullets and Numbering

- 1  
2  
3  
4  
5  
6  
7  
8  
9  
10  
11  
12  
13  
14  
15  
16  
17  
18  
19  
20  
21  
22  
23  
24  
25  
26  
27  
28  
29  
30  
31  
32  
33  
34  
35  
36  
37  
38  
39  
40  
41  
42  
43  
44  
45  
46  
47  
48  
49  
50  
51  
52  
53  
54  
55  
56  
57  
58  
59  
60
- 13 G. Ritzhaupt, J. P. Devlin, *Journal of Physical Chemistry*, 1991, **95(1)**, 90.  
14 R. H. Smith, M.T. Leu L. F. Keyser, *Journal of Physical Chemistry*, 1991, **95(15)**,  
5924.  
15 M. A. Tolbert, B. G. Koehler, A. M. Middlebrook, *Spectrochimica Acta Part A*,  
1992, **48A(9)**, 1303.  
16 T. L. Tso, M.-T. Leu, *Analytical Sciences*, 1996, **12(4)**, 615.  
17 B. G. Koehler, *International Journal of Chemical Kinetics*, 2001, **33(5)**, 295.  
18 K. D. Beyer, A. R. Hansen, *Journal of Physical Chemistry A*, 2002, **106(43)**, 10275  
19 H. Grothe, C. E. Lund-Myhre, C. J. Nielsen, *Journal of Physical Chemistry A*, 2006,  
**110**, 171.  
20 N. Barton, B. Rowland, J. P. Devlin, *Journal of Physical Chemistry*, 1993, **97(22)**,  
5848.  
21 J. Koller, D. Hadzi, *Journal of Molecular Structure*, 1991, **48A(9)**, 1303.  
22 R. Escribano, M. Couceiro, P. C. Gomez, E. Carrasco, M.A. Moreno, V. J. Herrero,  
*Journal of Physical Chemistry*, 2003, **107(5)**, 651.  
23 H. Tizek, E. Knoezinger, H. Grothe, *Phys. Chem. Chem. Phys.*, 2002, **4(20)**, 5128.  
24 R.G. Hynes, M.A. Fernandez, R.A. Cox, *J. Geophys. Res.*, 2002, **107**, 4797.  
25 M. Staikova, D.J. Donaldson, *Phys. Chem. Chem. Phys.*, 2001, **3**, 1999.  
26 P.R. McCurdy, W.P. Hess, S.S. Xantheas, *J. Phys. Chem. A*, 2002, **106**, 7628.  
27 S. Peil, S. Seisel, O. Schrems, *Journal of Molecular Structure*, 1995, **348**, 449.  
28 H. Yang, B. J. Finlayson-Pitts, *Journal of Physical Chemistry A*, 2001, **105(10)**,  
1890.  
29 M. Sato, O. Setokuchi, K. M. T. Yamada, T. Ibusuki, *Vibrational Spectroscopy*,  
2003, **31(2)**, 167.  
30 H. Reinhardt, M. Fida, R. Zellner, *Journal of Molecular Structure*, 2003, **661-662**,  
567.  
31 T.G. Koch, N.S. Homes, T.B. Roddis, J.R. Sodeau, *J. Chem. Soc. Faraday Trans.*  
1996, **92**, 4787.  
32 T.G. Koch, A.B. Horn, M.A. Chesters, M.R.S. McCoustra, J.R. Sodeau, *J. Phys.*  
*Chem.* 1995, **99**, 8362.  
33 A. M. Middlebrook, B. S. Berland, S. M. George, M. A. Tolbert, O. B. Toon,  
*Journal of Geophysical Research*, 1994, **99(D12)**, 25655.  
34 R. D. Poshusta, D. C. Tseng, A. C. Hess, M. I. Maureen, *Journal of Physical*  
*Chemistry*, 1993, **97(28)**, 7295.  
35 G. Toth, *Journal of Physical Chemistry A*, 1997, **101(47)**, 8871.  
36 D. Fernandez, V. Botella, V. J. Herrero, R. Escribano, *Journal of Physical Chemistry*  
*B*, 2003, **107(38)**, 10608.  
37 D. Fernandez-Torre, R. Escribano, T. Archer, J. M. Pruneda, E. Artacho, *Journal of*  
*Physical Chemistry A*, 2004, **108(47)**, 10535.  
38 D. Fernandez-Torre, R. Escribano, V.J. Herrero, B. Mate, M. A. Moreno, I. K.  
Ortega, *Journal of Physical Chemistry B*, 2005, **109(38)**, 18010.  
39 M. Walker, C. A. Morrison, D. R. Allan, *Physical Review B: Condensed Matter and*  
*Materials Physics*, 2005, **72(22)**, 224106/1.  
40 N. Lebrun, F. Mahe, J. Lamiot, M. Foulon, J. C. Petit, D. Prevost, *Acta*  
*Crystallographica Section B: Structural Science*, 2001, **B57(1)**, 27.  
41 H. Tizek, E. Knoezinger, H. Grothe, *PCCP*, 2004, **6**, 972.  
42 F. A. Miller, B. M. Harney, *Appl. Spectrosc.* 1970, **24**, 291.  
43 D. Colognesi, M. Celli, F. Cilloco, R. J. Newport, S. F. Parker, V. Rossi-Albertini, F.  
Sacchetti, J. Tomkinson, M. Zoppi, *Appl. Phys. A* 2002, **74 [Suppl.]**, S64.  
44 <http://www.isis.stfc.ac.uk/>

← --- Formatted: Bullets and Numbering

- 1  
2  
3  
4  
5  
6  
7  
8  
9  
10  
11  
12  
13  
14  
15  
16  
17  
18  
19  
20  
21  
22  
23  
24  
25  
26  
27  
28  
29  
30  
31  
32  
33  
34  
35  
36  
37  
38  
39  
40  
41  
42  
43  
44  
45  
46  
47  
48  
49  
50  
51  
52  
53  
54  
55  
56  
57  
58  
59  
60
- 45 [K. Ji, \*Dissertation, L'Universit  de Paris VII, 1994.\*](#)
- 46 [S. U. Pickering, \*J. Chem. Soc.\*, 1893, \*\*63\*\*, 436.](#)
- 47 [N. LeBrun, F. Mahe, J. Lamiot, M. Foulon, J. C. Petit, \*Acta Crystallographica Section C: Crystal Structure Communications\*, 2001, \*\*C57\*\*, 1129.](#)
- 48 M. Walker, C. R. Pulham, C. A. Morrison, D. R. Allan, W. G. Marshall, *Phys. Rev. B* 2006, **73**, 224110/1.
- 49 J. Potier, A. Potier, *C. R. Acad. Sci. Paris* 1956, **242**, 1474.
- 50 M. Pham Thi, M. H. Herzog-Cance, A. Potier, J. Potier, *J. Raman Spectrosc.* 1981, **11**(2), 96.
- 51 D. R. Allan, W. G. Marshall, D. J. Fancis, I. D. H. Oswald, C. R. Pulham, C. Spanswick, *Dalton Trans.* 2010, **39**, 3736.
- 52 W. Dmowski, T. Egami, K. E. Swider-Lyons, C. T. Love,; D. R. Rolison, *J. Phys. Chem. B* 2002, **106**, 12677.
- 53 A. A. Levchenko, A. I. Kolesnikov, N. L. Ross, J. Boerio-Goates, B. F. Woodfield, G. Li, A. Navrotsky, *J. Phys. Chem. A* 2007, **111**, 12584.
- 54 E. C. Spencer, A. A. Levchenko, N. L. Ross, A. I. Kolesnikov, J. Boerio-Goates, B. F. Woodfield, A. Navrotsky, G. Li, *J. Phys. Chem. A* 2009, **113**, 2796.
- 55 S. F. Parker, K. Refson, A.C. Hannon, E. Barney, S.J. Robertson, P. Albers, *J. Phys. Chem. C* 2010, **114**, 14164.
- 56 P. C. H. Mitchell, S. F. Parker, A. J. Ramirez-Cuesta, J. Tomkinson, *Vibrational spectroscopy with neutrons, with applications in chemistry, biology, materials science and catalysis*, World Scientific: Singapore, 2005.
- 57 A. J. Ramirez-Cuesta, *Comp. Phys. Comm.* 2004, **157**, 226.
- 58 R. Escribano, D. Fern andez-Torre, V. J. Herrero, B. Mart n-Llorente, B. Mat , I. K. Ortega, H. Grothe, *Vibr. Spectr.* 2007, **43**, 254.
- 59 R. Savoie, P. A. Gigu re, *J. Chem. Phys.*, 1964, **41**(9), 2698.
- 60 M. Hsinjui Kuo, A. David, N. Kamelamela, M. White, M. J. Shultz, *J. Phys. Chem C*, 2007, **111**, 8827.
- 61 R. Bianco, S. Wang, J. T. Hynes, *J. Phys. Chem. A*, 2008, **112**, 9467.
- 62 [H. Grothe, H. Tizek, I. Ortega, \*Faraday Discussion\*, 2008, \*\*137\*\*, 223.](#)

Formatted: Bullets and Numbering

Formatted: Bullets and Numbering

Deleted: ¶

Formatted: Bullets and Numbering

**Captions to figures:**

**Fig.1:** Projection of the crystal structure of NAM on the [001]-plane. This structure was calculated by refinement of the observed X-ray diffraction result. NAM consists of separated and corrugated two-dimensional layers.<sup>40</sup>

**Fig.2 a)** (1) X-ray diffractogram of an amorphous sample with  $x=0.5$  at  $T \leq 125$  K. (2) [X-ray diffractogram of](#) the same sample after annealing to 180K. The bar graph at top shows calculated reflections of NAM. SC indicates reflections of the sample carrier and the window.

**Fig.2 b)** (1) [FTIR-spectrum of amorphous NAM at 125 K.](#) (2) [Spectra of the same sample after crystallization at 180 K, and \(3\) annealed at 200 K, respectively.](#)

**Fig.3:** X-ray diffractogram of 54 mol% nitric acid at 180 K, 200 K and 210 K. A reflection at  $25.5^\circ$  indicates pure nitric acid and is shaded in grey (and labelled NA). It disappears above the eutectic temperature. A reflection at  $15.9^\circ$  is an impurity of  $\alpha$ -NAD and is marked with "D".

**Fig.4:** INS spectra of NAM evolving from an amorphous phase of 50 mol% nitric acid through annealing. The spectrum (1) shows the amorphous nitric acid ice mixture at 20 K as deposited before annealing. The spectrum (2) is taken after annealing to 180 K. Spectrum (3) is a calculated spectrum for NAM.

**Fig.5:** Comparison of the low frequency range spectra of NAM by Raman (3) and INS (2), both experimental, and IR, calculated (1).

**Fig. 6:** [ESEM pictures](#) of NAM: (a) amorphous sample at  $T \leq 125$  K, (b) crystalline sample at  $T=180$  K, after 10 min annealing time, (c) same sample and same conditions but [after](#) 20 min annealing [time](#), (d) as before but [after](#) 30 min annealing time.

**Table 1.** Low frequency vibrations (in  $\text{cm}^{-1}$ ) of NAM

INS <sup>a</sup>	IR <sup>b</sup>	Raman <sup>c</sup>	INS <sup>d</sup>	Assignment <sup>e</sup>
59		58		
70		75		
90		86		
		101		
124		118	112	
135		129		
154		143		
162			164	
203	195		206	Tz
216				
238	234			
249	268		246	Ty
300	304			
318	320(sh)		321	Tx+Tz
387				
421				

<sup>a</sup> INS data from this work, <sup>b</sup> IR calculations by Escribano et al.<sup>55</sup>, <sup>c</sup> Raman data by Grothe et al.<sup>19</sup>, <sup>d</sup> INS data from Janik et al.<sup>4</sup>, <sup>e</sup> assignments by Janik et al.<sup>4</sup>

**Table 2:** Vibrational spectroscopy data of NAM in the mid-IR region (in  $\text{cm}^{-1}$ )

INS <sup>a</sup>	IR <sup>b</sup>	IR <sup>c</sup>	IR <sup>d</sup>	IR <sup>e</sup>	Raman <sup>f</sup>	INS <sup>g</sup>	Assignment <sup>h</sup>
603							
673		675	670	680			(H <sub>3</sub> O <sup>+</sup> ) tors.
	702	700		702			$\nu_L$ (H <sub>3</sub> O <sup>+</sup> )
718	721	723	723	722			$\nu_4$ (NO <sub>3</sub> <sup>-</sup> ) $\delta_{\text{as}}$
	735	737	738	735			$\nu_4$ (NO <sub>3</sub> <sup>-</sup> ) $\delta_{\text{as}}$
750						758	(H <sub>3</sub> O <sup>+</sup> )Rz+Ry
770	780			775			
798	814	815	816	813			$\nu_2$ (NO <sub>3</sub> <sup>-</sup> ) $\delta_s$
877							
926							
969							calc.(NO <sub>3</sub> <sup>-</sup> ) $\nu_1$
					1044		
					1055		
1103	1102						
1114				1115			$\nu_2$ (H <sub>3</sub> O <sup>+</sup> ) $\delta_s$
1131	1135	1135	1134				
	1279			1260			$\nu_3$ (NO <sub>3</sub> <sup>-</sup> ) $\nu_{\text{as}}$
1314				1316			$\nu_3$ (NO <sub>3</sub> <sup>-</sup> ) $\nu_{\text{as}}$
1327							
1402		1386	1361				
1423							
1437							
1459							
1669	1674	1680	1671	1671			$\nu_4$ (H <sub>3</sub> O <sup>+</sup> ) $\delta_{\text{as}}$

<sup>a</sup>) INS data from this work, <sup>b</sup>) IR data by Ritzhaupt and Devlin<sup>13</sup>, <sup>c</sup>) IR data by Savoie and Giguere<sup>56</sup>, <sup>d</sup>) IR data by Bethell and Sheppard<sup>2</sup>, <sup>e</sup>) IR data by Smith et.al.<sup>14</sup>, <sup>f</sup>) Raman data by Grothe et al.<sup>19</sup>, <sup>g</sup>) INS data by Janik et al.<sup>4</sup>, <sup>h</sup>) the assignments are summarised from the different sources mentioned in the table.

1  
2  
3  
4  
5  
6  
7  
8  
9  
10  
11  
12  
13  
14  
15  
16  
17  
18  
19  
20  
21  
22  
23  
24  
25  
26  
27  
28  
29  
30  
31  
32  
33  
34  
35  
36  
37  
38  
39  
40  
41  
42  
43  
44  
45  
46  
47  
48  
49  
50  
51  
52  
53  
54  
55  
56  
57  
58  
59  
60

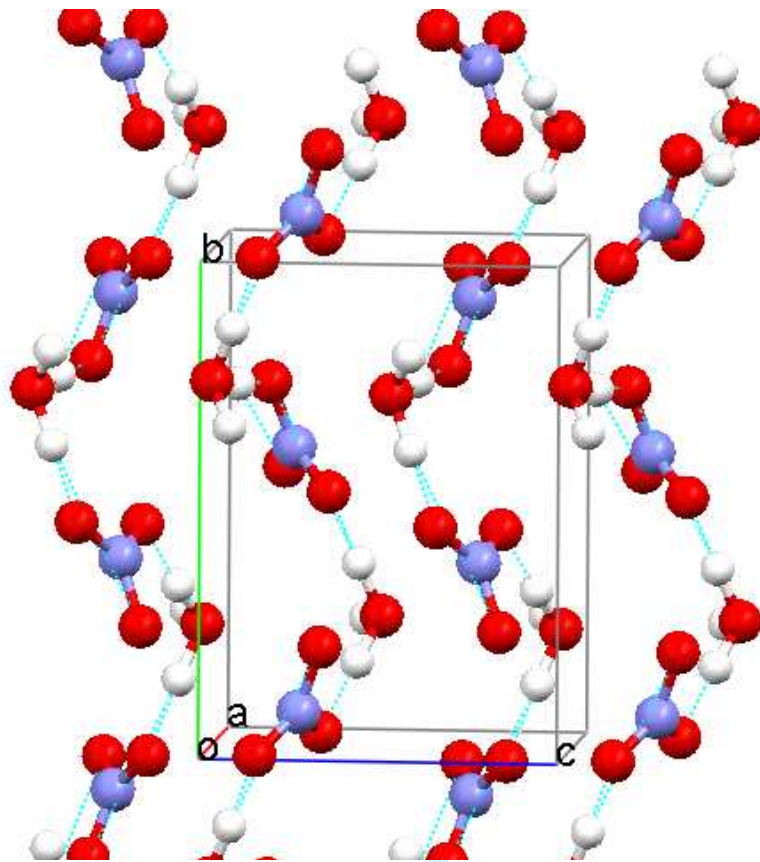


Figure 1

View Only

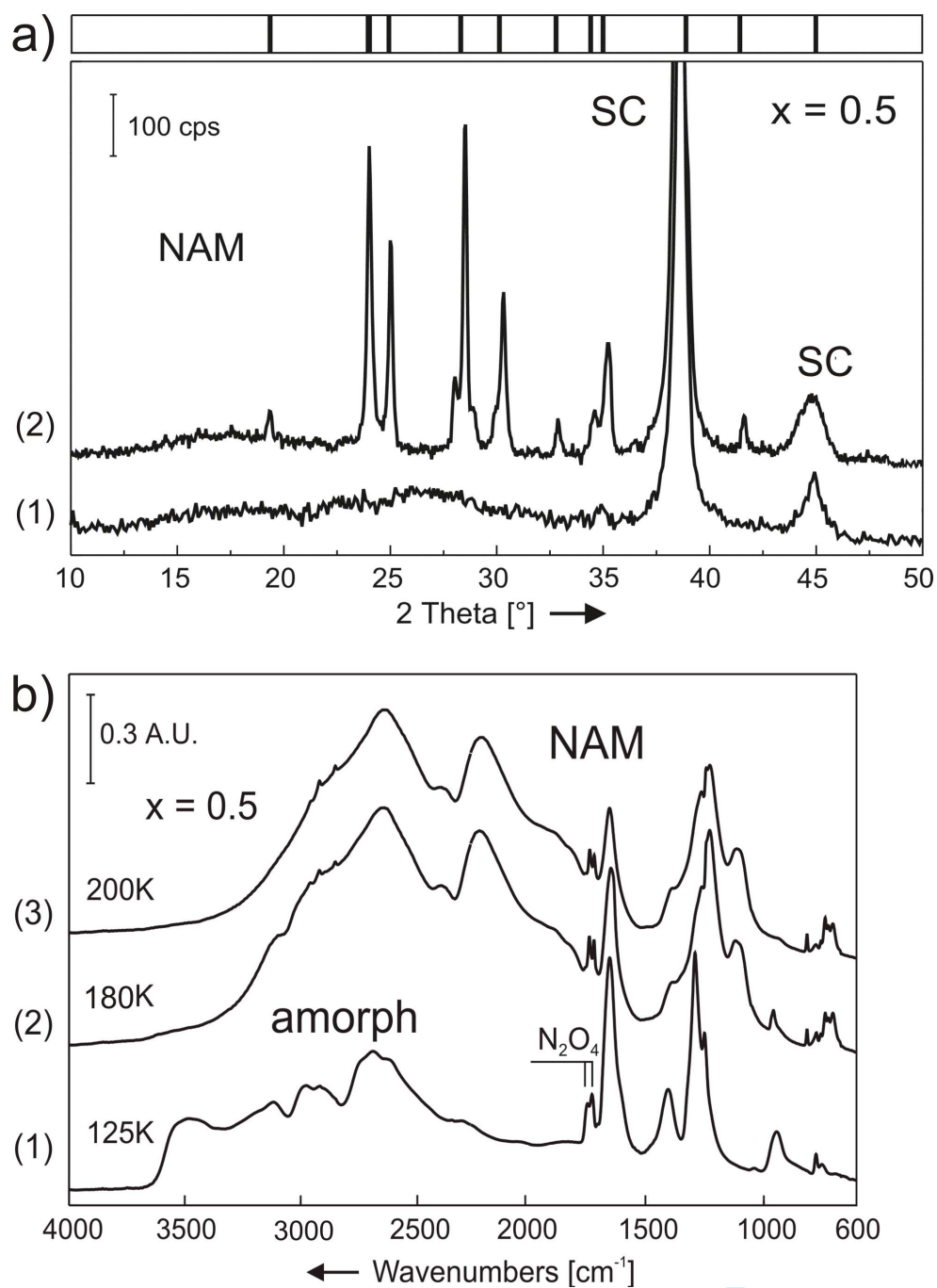


Figure 2

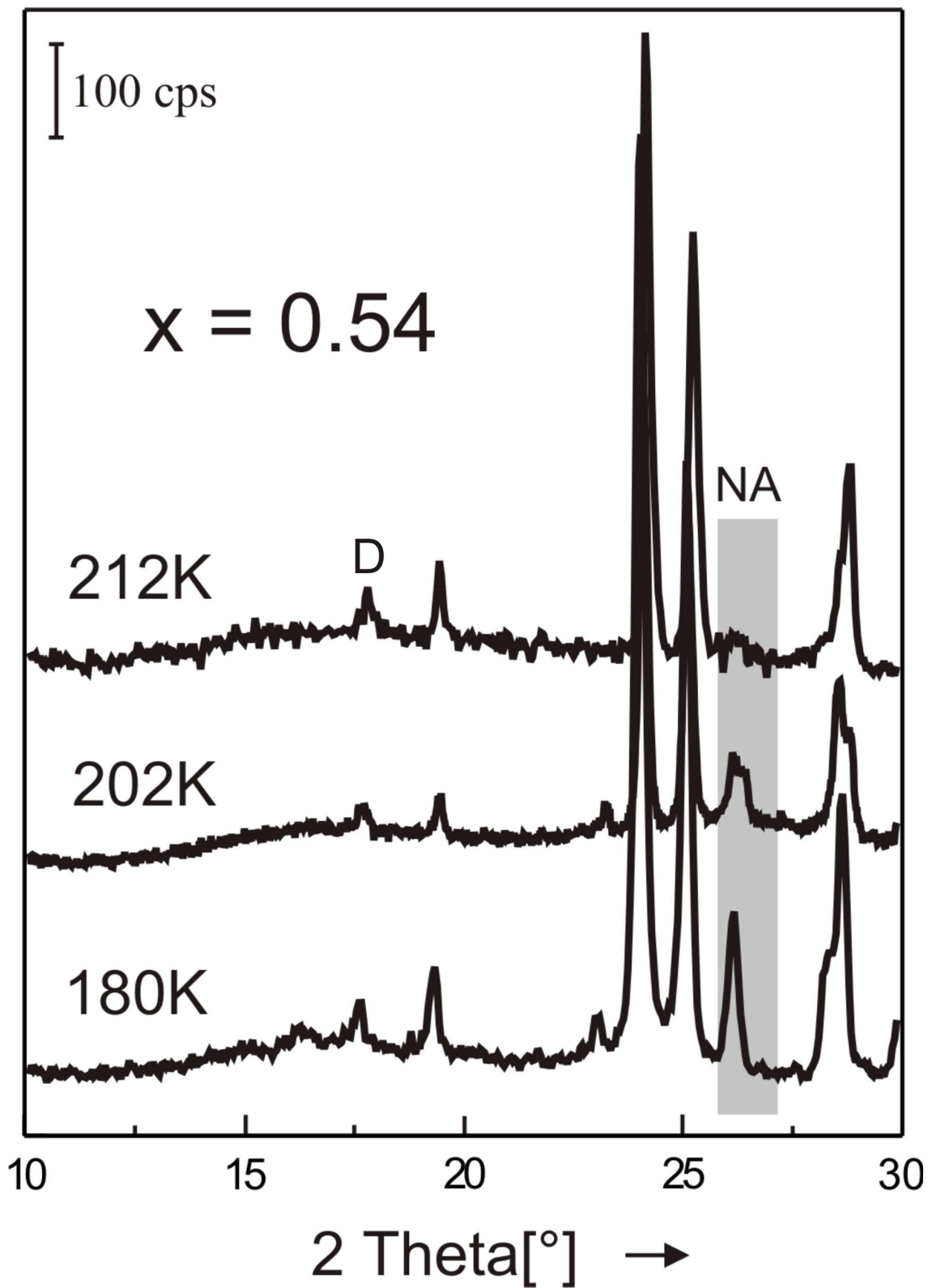


Figure 3

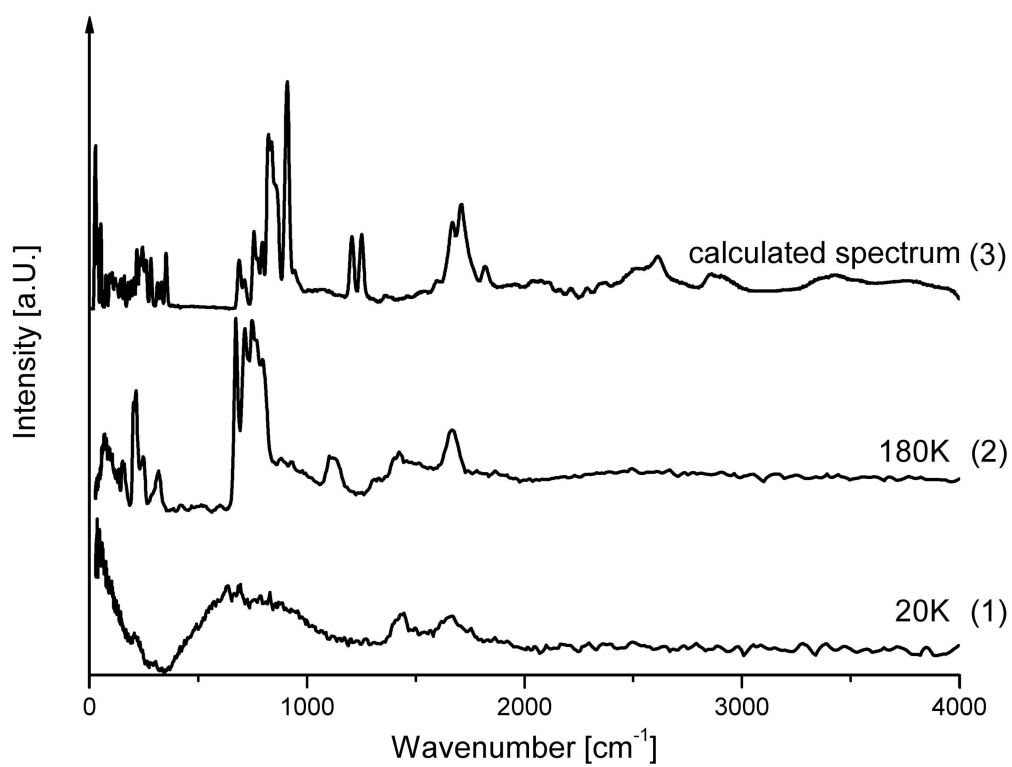


Figure 4

1  
2  
3  
4  
5  
6  
7  
8  
9  
10  
11  
12  
13  
14  
15  
16  
17  
18  
19  
20  
21  
22  
23  
24  
25  
26  
27  
28  
29  
30  
31  
32  
33  
34  
35  
36  
37  
38  
39  
40  
41  
42  
43  
44  
45  
46  
47  
48  
49  
50  
51  
52  
53  
54  
55  
56  
57  
58  
59  
60

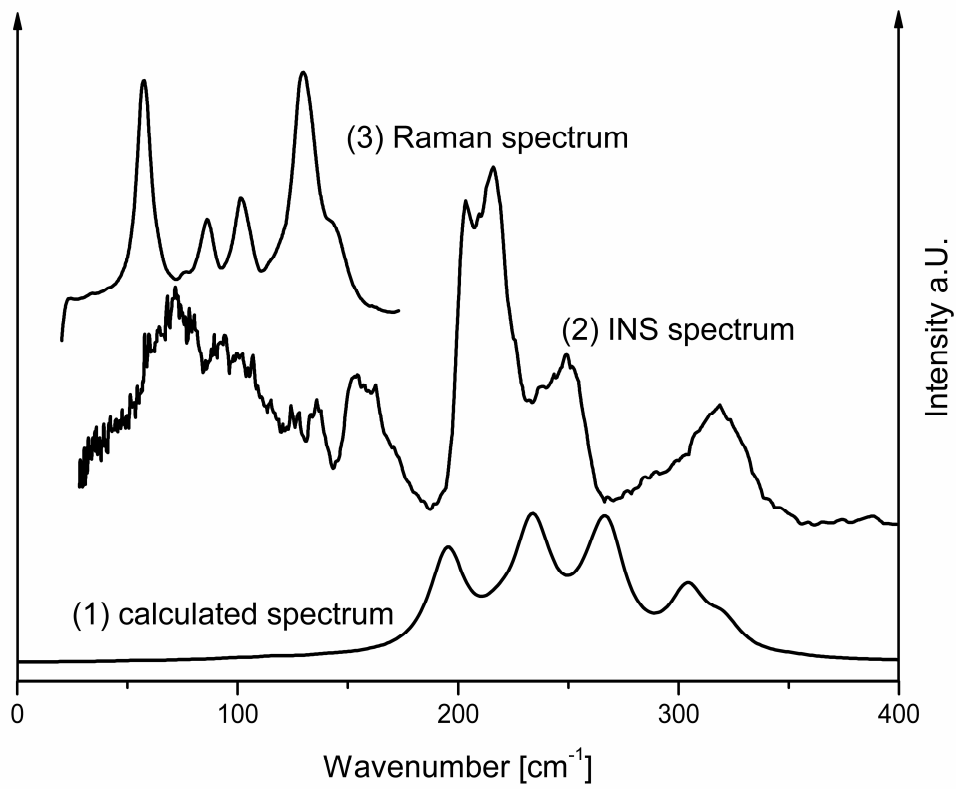


Figure 5

Review Only

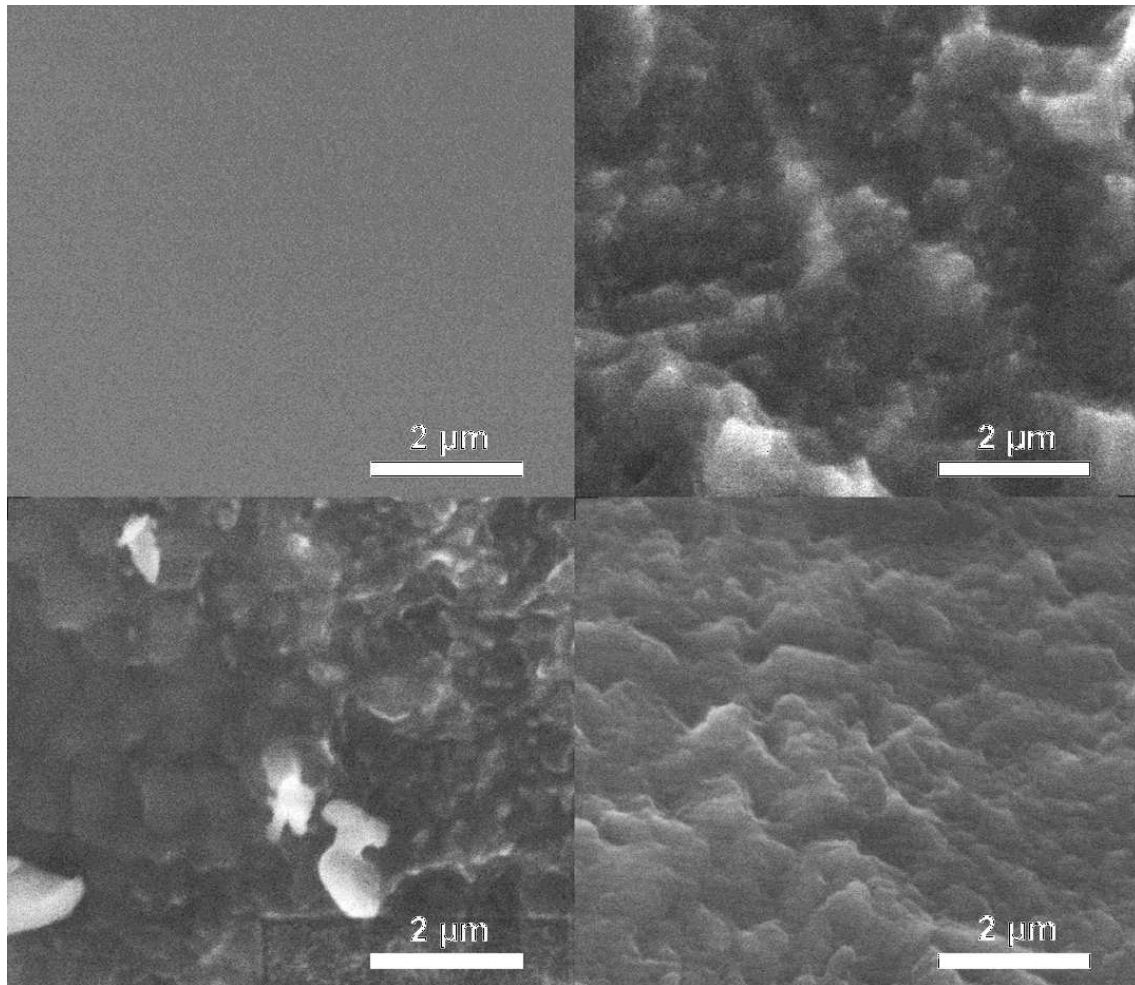


Figure 6